Visibility-Based Persistent Monitoring of Piecewise Linear Features on a Terrain Using Multiple Aerial and Ground Robots

Parikshit Maini, *Member, IEEE*, Pratap Tokekar, and P. B. Sujit, *Senior Member, IEEE*

***Abstract*— Persistent monitoring on terrains using mobile robotic sensors requires coordinated planning. Terrain features add visibility obstacles and limited fuel capacity of aerial robots leads to range restrictions that make the problem challenging. We address the visual-monitoring problem on piecewise linear features within a terrain using multiple mobile robots for persistent operations. The planner must account for visual coverage, refueling aerial robots during the mission, and placement of refueling depots while also utilizing the available sensor diversity to minimize overall costs for the monitoring mission. Building on previous works on visibility in specific classes of polygons and fuel-constrained routing, we develop a discrete representation of the problem that allows the design and application of discrete optimization techniques to find optimal solutions. We develop a mixed-integer linear programming (MILP) formulation and discuss a branch-and-cut implementation to compute exact solutions. We also develop a construction heuristic based on the idea of competitive construction of robot paths using a step-increment strategy. We report the results from computational simulations and illustrate proof of concept using experiments on real robots.**

***Note to Practitioners*—This article is motivated by the need to perform persistent monitoring in applications, such as border patrol and perimeter surveillance. Unmanned aerial and ground robots can be used to perform these activities uninterruptedly. However, aerial robots have limited fuel capacity and need periodic refueling. Hence, the number of refueling depots and their placement within the environment also affects the monitoring task. Also, due to terrain variation, robots are subject to limited visibility. Therefore, we need to consider refueling constraints and terrain visibility aspects while planning optimal routes for the robots to perform visual monitoring. In this article, we present a general optimal routing formulation to compute exact solutions. We also present a fast heuristic for real-time applications that produce feasible solutions. The algorithms are validated in simulations. We also show a proof of concept using experiments in limited outdoor settings.**

***Index Terms*— Mixed-integer linear programming (MILP), multi-robot systems, path planning, persistent monitoring, visibility.**

Manuscript received May 7, 2020; revised July 16, 2020; accepted July 28, 2020. This article was recommended for publication by Associate Editor C. K. Ahn and Editor D. O. Popa upon evaluation of the reviewers' comments. This work was supported in part by the National Science Foundation under Grant 1566247 and in part by Engineering and Physical Sciences Research Council (EPSRC) Grant EP/P02839X/1. The work of Parikshit Maini was supported in part by the TCS Ph.D. Fellowship and in part by IIIT Delhi. *(Corresponding author: P. B. Sujit.)*

Parikshit Maini is with the Department of Computer Science and Engineering, University of Minnesota, Minneapolis, MN 55455 USA (e-mail: pmaini@umn.edu).

Pratap Tokekar is with the Department of Computer Science, University of Maryland, College Park, MD 20742 USA (e-mail: tokekar@umd.edu).

P. B. Sujit is with the Department of Electrical Engineering and Computer Science, Indian Institute of Science Education and Research Bhopal (IISERB), Bhopal 462066, India (e-mail: sujit@iiserb.ac.in).

This article has supplementary downloadable material available at http://ieeexplore.ieee.org, provided by the authors.

Color versions of one or more of the figures in this article are available online at http://ieeexplore.ieee.org.

Digital Object Identifier 10.1109/TASE.2020.3014949

I. Introduction

VISUAL monitoring using autonomous mobile robots has been transformative in applications, such as intelligence, surveillance, and reconnaissance operations (ISRs) [1], [2], disaster management [3], [4], and structural monitoring [5], [6]. In this context, the utility of cooperative aerial and ground robot systems for monitoring tasks is an active area of research and has garnered a lot of interest from the research community over the last decade. In this article, we study the use of a cooperative heterogeneous robot system for persistent monitoring on a terrain. Applications, such as rail-track monitoring [5], [7], power-line inspection [8], border and highway patrol [9], and river monitoring [10], involve extended features that may span several kilometers in length and often witness terrain variability in terms of altitude. This restricts the visibility of robotic sensors and requires intricate planning algorithms for successful mission completion. We model terrain features such as roads, borders, and pipelines as piecewise linear ([10] and [11] also use similar models) and address the problem of persistent monitoring of such features using a cooperative system of aerial and ground robots (see Fig. 1). This class of problems is combinatorial in nature and is computationally intensive.

There exists literature that addresses cooperative routing for mobile robots [12]–[15], persistent monitoring [1], [13], [14], [16]–[20], and other related problems. However, this work fills a gap in the literature and addresses the visibility-based persistent monitoring problem for piecewise linear features on a terrain using autonomous aerial and ground robots. The problem includes negotiating visibility and fuel restrictions, joint planning for a cooperative system of heterogeneous robots, and the placement of refueling depots that comes into significance due to the requirements of a persistent mission. We model the mission cost to include one-time setup costs for refueling depots and operating costs for the robotic agents. The solution involves geometric modeling for visibility computation within the terrain, selection of a guard set, fuel-constrained route planning for robotic agents, and placement of refueling depots on the terrain to ensure mission feasibility while minimizing

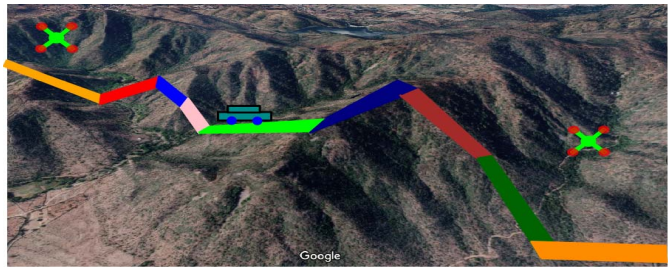

Fig. 1. Example scenario of a piecewise linear feature (colored segments) on a terrain where a team of robots consisting of two aerial vehicles and one ground vehicle is monitoring.

the total cost. We use the terms tour, route, and sequence interchangeably throughout the rest of the text.

The rest of this article is organized as follows. Section II reviews the related work and contextualizes the technical contributions of this work. Section III discusses preliminaries on terrain model, robot models, persistent monitoring, and the placement of refueling depots. Section IV describes the application scenario and establishes the problem statement. Section V develops the mixed-integer linear programming (MILP) and heuristic solution methods. Section VI describes the computational simulations, including setup, instance generation, examples, and results. Section VII describes the experiments used to illustrate the proof of concept. Section VIII concludes this article and identifies future research directions.

II. Related Work

Determining tours for a robot to fully observe a given space is popularly known as the watchman routing problem (WRP) [21], [22]. WRP is a well-studied problem. The simple version of WRP in a polygon without holes may be solved in polynomial time [22]; for polygon with holes, Mitchell [23] devised an approximation algorithm with a $\log^2 n$-approximation factor and showed that the approximation factor cannot be improved beyond $c \log n$ for some constant $c > 0$. In the multiple watchmen (n-WRP) version [24], the goal is to compute tours for n robots (watchmen) to cover the environment. Carlsson *et al.* [24] show that n-WRP is NP-hard. Due to the inherent complexity of the problem, practical solution approaches, including decoupled viewpoint selection followed by robot routing [25] and self-organizing map heuristics [26], have been developed. There have also been efforts to design algorithms for restricted polygon domains: spiral polygons [27], histograms [28], and street polygons [17], [24]. Exact [27], [28] and approximate [17] solution approaches for the n-WRP have been designed for these special polygonal domains by exploiting their structural characteristics. All of these approaches address the case of the homogeneous robot. In this work, we address a persistent version of n-WRP to monitor a piecewise linear feature on a terrain and extend the current state of the art by admitting the use of heterogeneous robotic sensors.

Persistent monitoring using mobile robots is also a well-studied problem in the literature. Variations of the persistent monitoring problem for a single robot have been addressed in [18] and [29]–[31]. Alamdari *et al.* [18] introduced the idea of the kernel of an infinite walk as a closed walk that may be repeated to find an infinite walk for a mobile robot. Manyam *et al.* [1] addressed the homogeneous multirobot persistent monitoring problem in the context of a data delivery application with constraints on data freshness. Mathew *et al.* [32] solved a scheduling problem for mobile recharging stations to rendezvous with aerial robots for a persistent monitoring application. Ghazzai *et al.* [4] developed a scheduling framework to optimize the battery capacity of aerial robots to visit spatially and temporally distributed targets. The use of mobile ground robots as mobile refueling nodes has been explored in [13], [14], [19], [20], and [33]. Lasla *et al.* [6] developed an approach to utilize public transport to extend the operational range of aerial robots and optimize energy consumption in a smart city scenario. The problem of placement of refueling depots is complementary to persistent monitoring and significantly affects the mission cost. Maini *et al.* [13], Yu *et al.* [14], Mathew *et al.* [32], and Yu *et al.* [33] addressed different versions of the fuel-constrained routing problem for aerial robots and used mobile refueling stations operating on the ground. They developed methods to determine rendezvous sites and time intervals to refuel the aerial robots and extend their range of operation. The work of Funke *et al.* [34] addresses the problem of placement of recharging depots for electric automobiles, ensuring that they can travel long distances with minimal detours for recharging.

Contributions: In this work, we address both, route planning and placement of refueling depots, for persistent monitoring using a diverse set of robotic agents. The contributions of this work are as follows.

1) We address the persistent monitoring problem for piecewise linear features on altitude varying terrains using a heterogeneous set of ground and aerial mobile robotic sensors.
2) Our solution approach considers robot path planning and refueling depot placement as a coupled problem and determines solutions to both problems while optimizing the overall mission cost.
3) We develop an MILP formulation for the persistent monitoring problem and discuss a branch-and-cut-based implementation.
4) We develop a construction heuristic called δ-search based on the competitive construction of robot paths using a step-increment strategy.
5) We validate and compare our methods using large-scale computational simulations.
6) We also conduct outdoor experiments using multiple aerial and multiple ground robots to establish proof of concept.

A preliminary version of this article was presented in [35] and [36]. This article includes the framework from the preliminary version and generalizes it. In this article, we extend the framework using a generalized MILP formulation for the monitoring problem, develop a construction heuristic (δ-search), and experimentally demonstrate using two UAVs and two ground rovers.

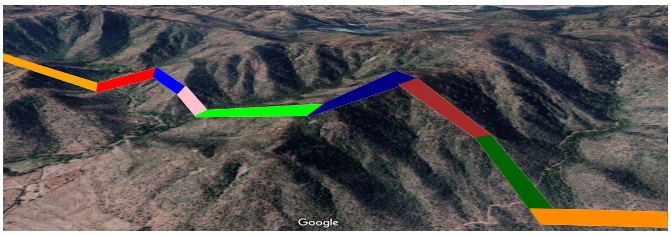

(a)

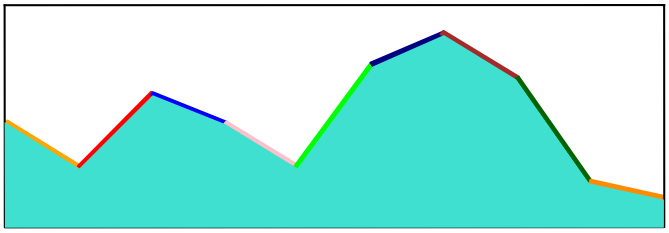

(b)

Fig. 2. (a) Piecewise linear feature within a terrain may be straightened out to build a 1.5-D model. (b) 1.5 terrain of (a) with the individual edges of the features having same color.

III. Preliminaries

We discuss some preliminary ideas needed to develop our solution methods in this section. Specifically, we formalize the visibility-based model of the terrain and establish the definitions used in the rest of this article. We also describe the chain visibility property and the robot model used.

A. Terrain Model

We use the model and terminology for terrain features as defined in [35]. For completeness, we give an overview here. The environmental feature to be monitored is modeled as a 1.5-D structure. As shown in Fig. 2, a piecewise linear feature within a terraineous environment may be straightened out in one dimension to build a 1.5-D model. The 1.5-D representation of a feature is x-monotone and is characterized by terrain points and reflex points [see Fig. 3(a)].

Definition 1 (Terrain Point): A terrain point is any point on the surface of the terrain that observes a change in slope.

Consider a 1.5-D terrain as shown in Fig. 3(a). The figure shows 12 terrain points marked using an asterisk symbol.

Definition 2 (Reflex Point): A reflex point is a terrain point where the slope decreases while going in the left-to-right direction on the terrain.

The set of reflex points is a subset of the set of terrain points. Fig. 3(a) shows seven reflex points on the terrain, marked using a red asterisk symbol.

Definition 3 (Chain Visibility): A curve C and a set of points X in 2-D are said to be chain visible if for each point $x \in X$, the intersection of the visibility polygon, i.e., space that has an unrestricted view of x, and C is either an empty set or a connected chain [17].

Fig. 3(b) shows the visibility polygon for a point x on the terrain. Examples of chain visible pairs include street polygons and collapsed watchman routes [37], points on a 1.5-D terrain, and fixed altitude paths [17]. In our case, the fixed altitude path [line C in Fig. 3(b)] corresponds to the aerial robot flight altitude and the set of points X comprises points that lie on the terrain.

Definition 4 (Visibility Segment): The surface of a 1.5-D terrain between two consecutive reflex points forms a convex polyline and is called a visibility segment.

Fig. 3(c) shows a visibility segment marked as a blue colored line on the terrain. When the context is clear from the text, we use "segment" to refer to a "visibility segment." Each visibility segment is marked on the terrain by a left and a right reflex point.

Definition 5 (Visibility Region): The region on the constant-altitude flight path between the extended projections of the right edge of the left reflex point and left edge of the right reflex point of the visibility segment is defined as the visibility region of the given visibility segment.[1]

Visibility region of a segment is a continuous curve, and any point in the visibility region has an unobstructed view of the corresponding segment. Fig. 3(c) shows the visibility region of a segment on the terrain on the constant altitude flight path. It also shows the extended projections from the left and right reflex points of the segment that intersects with the chain visible curve to mark the visibility region. The continuity of the visibility region is attributed to the property of chain visibility between the constant altitude flight path and the terrain, and convexity of the visibility segment.

In the case of ground robots, we explicitly define the visibility region for a segment to be the segment itself. The visibility regions on ground robot paths also satisfy the condition that any point in the visibility region has an unobstructed view of the corresponding segment. This is true since each visibility segment is convex.

Definition 6 (Viewpoints): Left and right end points of a visibility region are referred to as the left and right viewpoints, respectively, of the corresponding visibility segment.

The intersection of the extended projections from the left and right reflex points of a segment, with the chain visible curve as shown in Fig. 3(c), marks the two viewpoints for the segment. Fig. 3(d) shows the left and right viewpoints for all visibility segments on the terrain.

B. Robot Model and System Assumptions

In this work, we are concerned with developing high-level route planning algorithms and, hence, do not consider robot kinematics and dynamics. Furthermore, the techniques developed here find application in offline planning within a static environment and do not consider communication between any of the robots during the monitoring task. We make the following system assumptions for ease of exposition.

1) We assume the availability of a robust point-to-point navigation and obstacle avoidance system on each robot, including the availability of localization estimates.
2) We assume ideal operating conditions and do not consider the effects of weather, wind, or material properties of the terrain. Furthermore, the terrain material

[1]In case of visibility obstructions, the projections are suitably adjusted to pass through the obstructing reflex point to compute the visibility region.

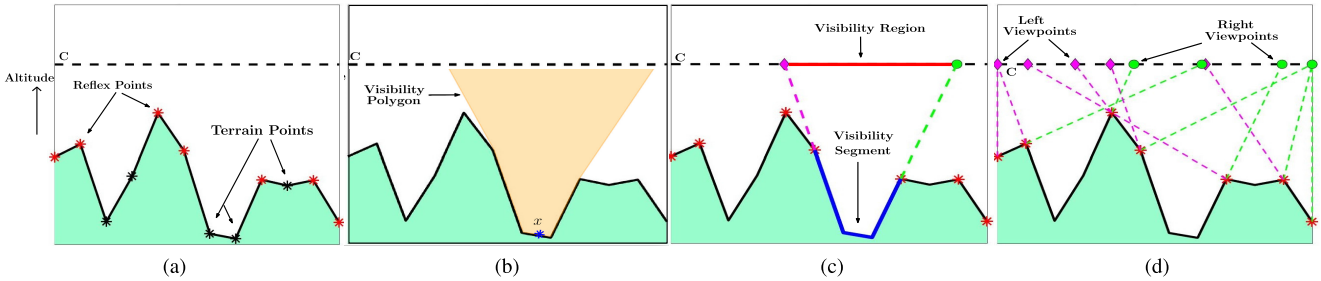

Fig. 3. (a) Terrain points, reflex points, and a fixed altitude path, C, chain visible with the terrain. (b) Visibility polygon corresponding to a point x on the terrain. (c) Visibility segment and its corresponding visibility region. (d) Left and right viewpoints for all visibility segments.

properties are considered to be uniform throughout the operational environment.

These assumptions are not restrictive and allow the modular development of high-level planning and coordination algorithms for mobile robots. Point-to-point navigation is usually performed by low-level controllers that directly interface with onboard sensors and actuators. The effect of environmental disturbances and variations is independent topics of research and outside but complementary to the scope of this study.

The aerial robot model used in this work is a multirotor-type vertical take-off and landing (VTOL) model with a given maximum fuel capacity. Aerial robots may have different fuel capacities and operate at different fixed altitudes with a constant individual airspeed. Assuming a constant rate of fuel consumption, regardless of the maneuver, and a constant speed for each robot, flight time, distance traveled, fuel consumed, and cost are proportional quantities and are used interchangeably. Furthermore, the operating cost of aerial robots is directly proportional to the Euclidean distance traversed and flight altitude. The ground robots are assumed to have infinite fuel availability and do not run out of fuel. The cost function for ground robot operation is proportional to the Euclidean distance traversed and slope of the terrain. We only consider fuel limitations for aerial robots since they usually operate under strong payload restrictions and each refueling operation entails a landing and take-off sequence leading to significant overhead costs.

C. Persistent Monitoring

To conduct persistent monitoring, a planner must compute an infinitely long monitoring route for each robot. Such an infinite sequence may exist in one of the following two forms: 1) a repetitive sequence and 2) a nonrepeating sequence. In this work, we restrict our search to repetitive sequences, in which a certain finite sequence is repeated infinitely many times to build an infinite sequence. Alamdari *et al.* [18] defined the repeating sequence as the kernel of an infinite sequence. The length of the kernel, i.e., the time taken to complete one execution of the kernel, determines the frequency of monitoring the terrain. The maximum time between two consecutive observations of any point on the terrain is upper bounded by the length of the kernel.

In the multirobot persistent monitoring problem, the kernel would comprise of a route for each robot such that each visibility segment on the terrain is covered by at least one robot. Furthermore, a robot may visit certain viewpoints multiple times within the kernel. Let the maximum number of times a robot visits a viewpoint within the kernel be κ. In our setup, the monitoring takes place along an x-monotone curve, and any point on a robot's path that does not lie on the left or the right extreme would need to be visited twice—once going forward and once returning back. A viewpoint on one of the extremes would be visited only once. Hence, the smallest feasible value of κ is two. Except in the case where one of the viewpoints lies directly above a take-off point (starting location or a refueling depot), it is straightforward to show that for any path that visits a viewpoint more than twice, there exists a shorter equivalent path that visits the viewpoint at most two times. For this reason, we set $\kappa = 2$ in our setup.

In the scenario, when a viewpoint exists directly above a take-off location, a robot may visit the viewpoint more than two times. While this does not pose any problems in field operations, even a small increase in the value of κ significantly increases the size of the search space (we discuss additional details on κ in Section V-A). To address this, we add a preprocessing step, which takes linear time, to check whether a viewpoint lies directly above the starting point or any of the candidate refueling depot opening sites. If such a viewpoint is found, a small noise may be added to the take-off location. Such a small deviation does not affect field operations since take-off platform space requirements are relatively insignificant due to the size of the aerial robots in consideration.

D. Refueling Depot Placement

A solution to the persistent monitoring problem must also decide on the placement of refueling depots in the environment. Both automated and manually operated depots for refueling or battery replacement in aerial robots incur additional resources, and hence, their number and placement need to be optimized. The placement of refueling depots and the planning of robot paths are complementary problems. While the refueling depot placement ensures reachability of viewpoints by aerial robots, the selection of viewpoints on a robot's path determines the subset of viewpoints that affect the placement of refueling depots. Too many refueling depots would result in wastage of resources, while too few would result in higher cost robot paths or potentially an incomplete mission, in a scenario where only aerial robots are available.

Existing works in the literature either assume that refueling depot locations are given [30], decouple route planning and placement of refueling depots/sites [13], [19], [20], [32], or setup refueling depots/sites at a subset of points visited by the aerial robot [14].

This work significantly extends the state of the art by jointly optimizing route planning for robots and the placement of refueling depots. We model the placement problem, on the lines of the classic facility location problem [38] where refueling depots must be opened at a subset of potential depot opening sites to ensure reachability of viewpoints. We develop a combined mathematical formulation to determine both robot paths and refueling depot placement while also accounting for associated costs in the optimization criteria.

IV. Problem Formulation

Consider an environment $\mathcal{E}$ as shown in Fig. 2 for a persistent monitoring application. The piecewise linear feature is represented as a 1.5-D terrain. Two types of robots are available: aerial robots with given fuel capacities and flight altitudes (greater than the highest point on the terrain) and ground robots that traverse on the terrain. Each individual flight altitude corresponds to a chain visible curve to the 1.5-D terrain. Let $\mathcal{C}$ be a set that comprises constant altitude flight paths and the 1.5-D terrain representation that corresponds to the paths for ground vehicles. Let $\mathcal{A}_c$ be the set of autonomous robots, ground or aerial, on the curve $c \in \mathcal{C}$. Then, $\mathcal{A} = \bigcup_{c\in\mathcal{C}} \mathcal{A}_c$ is the set of all robots. Also, let U_k^c be the fuel capacity and s_c^k be the starting location for the robot $k \in \mathcal{A}_c$. The fuel capacity for ground robots is assumed to be infinite. The starting location of an aerial robot is also considered a refueling depot and is also available to other aerial robots, if the aerial robot is used in the monitoring mission.

A planner must compute paths for robots in the set $\mathcal{A}$ to monitor, in combination, each of the visibility segments on the terrain. There also exist a set of refueling depot opening sites, $\mathbb{D}$, located on the terrain. A solution to the persistent monitoring problem must also determine the placement of refueling depots from the sites in $\mathbb{D}$, i.e., it must determine a subset of sites in $\mathbb{D}$ to open refueling depots. Each site $d \in \mathbb{D}$, where a refueling depot is opened, incurs a one-time depot opening cost. The aerial robots may use any of the opened refueling depots as computed by the path planner, to refuel during the mission.

To this end, we design a cost function that comprises of two components: 1) a maximum robot path cost and 2) sum of refueling depot opening costs for each opened depot. The first component adds the maximum operational cost (proportional to distance traveled/travel time) of a single robot, to the cost function. This component rewards simultaneous robot operation and prioritizes the length of the kernel of the persistent mission over individual robot operating costs. The second component corresponds to the one-time setup costs incurred in opening refueling depots. This component optimizes the number and placement of refueling depots setup in the environment. In such a scenario, the heterogeneous watchmen persistent routing problem on a terrain (HWPRPT) may be defined as follows.

Definition 7 (HWPRPT): Given a 1.5-D terrain and a set of ground and aerial robots with optical sensors, fuel limitations, and given operating altitudes, determine a placement of refueling depots in the environment and plan routes for the robots such that all points in the terrain are observed by at least one robot and the aerial robots never run out of fuel. The cost function, as given in (1), minimizes the sum of maximum robot path cost and refueling depot opening costs

$$\min \left\{ \max_{i\in\mathcal{A}} \text{cost}(\Pi_i) + \sum_{d\in\mathbb{D}} \beta(w_d) \right\} \tag{1}$$

where $\text{cost}(\Pi_i)$ is the cost of the path Π_i for robot i and $\beta(w_d)$ is the cost of opening a refueling depot at site $d \in \mathbb{D}$.

Note to Practitioners: By design, we do not minimize the total operating cost of the robots, and hence, the solutions may include overlapping paths for the robots operating at the same altitude. This is a direct repercussion of the min–max component of the objective function. In the context of our problem, if needed, the robot path overlaps can be removed in a simple postprocessing step by considering the paths pairwise and snipping at the point of first intersection of the paths when going in the left-to-right direction. The paths of both robots on the same side of the snipping point may be combined and assigned to one robot, and the paths of both robots on the other side of the snipping point may be combined and assigned to the other robot. This process does not increase the value of the objective function as defined by (1). We do not include this postprocessing in this work.

V. Solution Approach

We develop two solution methods: 1) an exact approach that builds on an MILP formulation for the problem and is implemented within a branch-and-cut framework and 2) a computationally efficient construction heuristic, named δ-search algorithm. The core idea of the heuristic is the competitive construction of routes for all robots while minimizing the step increase in the objective function value. In this section, we first establish the notation used in the solution methods and then describe the two solution methods.

Let ν be the set of visibility segments on the terrain. By virtue of the chain visibility property and the convexity of the segments, each segment is visible from every curve in $\mathcal{C}$ and has at most two distinct end points of the visibility region on each curve, referred to as the left and right viewpoints. Let $\mathcal{V}_c^L$ and $\mathcal{V}_c^R$ be the set of left and right viewpoints on the curve c, respectively (see Fig. 3). Let $\mathcal{V}_c = \mathcal{V}_c^L \bigcup \mathcal{V}_c^R$ be the set of all viewpoints on the curve $c \in \mathcal{C}$ and $\mathcal{V} = \bigcup_{c\in\mathcal{C}} \mathcal{V}_c$ be the set of all viewpoints over all curves in the set $\mathcal{C}$. $\mathcal{V}^L = \bigcup_{c\in\mathcal{C}} \mathcal{V}_c^L$ and $\mathcal{V}^R = \bigcup_{c\in\mathcal{C}} \mathcal{V}_c^R$ are defined similarly. $\mathcal{V}_c(v)$, $\mathcal{V}_c^L(v)$, $\mathcal{V}_c^R(v)$, $\mathcal{V}^L(v)$, and $\mathcal{V}^R(v)$ are subsets of viewpoints corresponding to the visibility segment v contained in the respective set. To quantify coverage and path costs, we define a visibility function and two cost functions as follows.

Definition 8 (Visibility Function): $\gamma_c(v) : \nu \rightarrow \wp(\mathcal{V}_c)$, where $\wp(x)$ is the power set of x, is defined for each

curve $c \in \mathcal{C}$. $\gamma_c(v)$ is the set of viewpoints on curve c that lies between the left and right end points of the visibility region for the segment v, and thus, $\gamma_c(v) \subseteq \mathcal{V}_c$. Also, $\gamma(v) = \bigcup_{c\in\mathcal{C}} \gamma_c(v)$.

Definition 9 (Cost Function 1): $\alpha_{ij}^c : V_c \times V_c \rightarrow \mathbb{R}^+$ returns the cost to travel from i to j on the curve $c \in \mathcal{C}$, where i and j belong to the set $V_c = \mathcal{V}_c \bigcup \mathbb{D}$.

Definition 10 (Cost Function 2): $\beta_d : \mathbb{D} \rightarrow \mathbb{R}^+$ defines the cost of opening a refueling depot at the site $d \in \mathbb{D}$.

A. MILP Formulation

We use the following sets of variables in the MILP formulation.

1) $x_{ij}^{\mathrm{ckl}_1 l_2}$, defined for each $c \in \mathcal{C}, k \in \mathcal{A}_c, i, j \in V_c$ and $l_1, l_2 \in \{1 \dots \kappa\}$. $x_{ij}^{\mathrm{ckl}_1 l_2} = 1$, if the kth vehicle on the cth curve visits the jth vertex along the edge (i, j) on c and 0 otherwise. l_1 and l_2 refer to the serial number of the current visit by the kth vehicle to i and j, respectively.
2) $z_{ij}^{\mathrm{ckl}_1 l_2}$, defined for each $c \in \mathcal{C}, k \in \mathcal{A}_c, i, j \in V_c$ and $l_1, l_2 \in \{1 \dots \kappa\}$. $z_{ij}^{\mathrm{ckl}_1 l_2}$ are real-valued decision variables that represent the amount of fuel consumed by the kth vehicle on the cth curve to visit the jth vertex along the edge (i, j) on c, from the most recently visited depot. l_1 and l_2 refer to the serial number of the current visit on the two vertices.
3) y_i^{ck} are binary variables defined for each $c \in \mathcal{C}$, $k \in \mathcal{A}_c, i \in V_c$. They take value 1 if the kth vehicle on the cth curve visits the ith vertex and 0 otherwise.
4) w_d are binary decision variables defined for each $d \in \mathbb{D}$. w_d mark the opened refueling depots at sites in $\mathbb{D}$.

For each $c \in \mathcal{C}$ and $\mathcal{P} \subseteq V_c$, let $\delta_c^+(\mathcal{P}) \equiv \{(i, j) : i \in \mathcal{P}, j \in V_c \setminus \mathcal{P}\}$ be the set of all outgoing edges from set $\mathcal{P}$ to $V_c \setminus \mathcal{P}$. We now give an expanded form of the objective function described in (1) to be used in the MILP formulation

$$\min \left\{ \left(\max_{c\in\mathcal{C},\ k\in\mathcal{A}_c} \sum_{l_1\in\{1\dots\kappa\}} \sum_{l_2\in\{1\dots\kappa\}} \sum_{i\in V_c} \sum_{j\in V_c} \alpha_{ij}^c \cdot x_{ij}^{\mathrm{ckl}_1 l_2} \right) + \sum_{d\in\mathbb{D}} \beta_d w_d \right\}. \quad (2)$$

The constraints used in the MILP are as follows.

Degree Constraints:

$$\sum_{l_2\in\{1\dots\kappa\}} \sum_{j\in V_c\setminus i} x_{ji}^{\mathrm{ckl}_2 l_1} - \sum_{l_2\in\{1\dots\kappa\}} \sum_{j\in V_c\setminus i} x_{ij}^{\mathrm{ckl}_1 l_2} = 0 \quad \forall c \in \mathcal{C},\ k \in \mathcal{A}_c,\ i \in V_c,\ l_1 \in \{1 \dots \kappa\} \quad (3)$$

$$\sum_{l_2\in\{1\dots\kappa\}} \sum_{j\in V_c\setminus i} x_{ji}^{\mathrm{ckl}_2 l_1} \leq 1 \quad \forall c \in \mathcal{C},\ k \in \mathcal{A}_c,\ l_1 \in \{1 \dots \kappa\},\ i \in \mathcal{V}_c \quad (4)$$

$$\sum_{l_3\in\{1\dots\kappa\}} \sum_{j\in V_c\setminus i} x_{ji}^{\mathrm{ckl}_3 l_1} - \sum_{l_3\in\{1\dots\kappa\}} \sum_{j\in V_c\setminus i} x_{ji}^{\mathrm{ckl}_3 l_2} \geq 0 \quad \forall c \in \mathcal{C},\ k \in \mathcal{A}_c,\ l_1, l_2 \in \{1 \dots \kappa\},\ l_2 = l_1 + 1,\ i \in V_c. \quad (5)$$

Visit Constraints:

$$y_i^{\mathrm{ck}} - \sum_{l_2\in\{1\dots\kappa\}} \sum_{j\in V_c\setminus i} x_{ji}^{\mathrm{ckl}_2 1} = 0 \quad \forall c \in \mathcal{C},\ k \in \mathcal{A}_c,\ i \in \mathcal{V}_c \quad (6)$$

$$y_d^{\mathrm{ck}} - x_{jd}^{\mathrm{ckl}_2 1} \geq 0 \quad \forall c \in \mathcal{C},\ k \in \mathcal{A}_c,\ d \in \mathbb{D},\ j \in V_c \setminus d,\ l_2 \in \{1 \dots \kappa\} \quad (7)$$

$$y_d^{\mathrm{ck}} - \sum_{l_2\in\{1\dots\kappa\}} \sum_{j\in V_c\setminus d} x_{jd}^{\mathrm{ckl}_2 1} \leq 0 \quad \forall c \in \mathcal{C},\ k \in \mathcal{A}_c,\ d \in \mathbb{D} \quad (8)$$

$$w_d - y_d^{\mathrm{ck}} \geq 0 \quad \forall c \in \mathcal{C},\ k \in \mathcal{A}_c,\ d \in \mathbb{D} \quad (9)$$

$$w_d - \sum_{c\in\mathcal{C}} \sum_{k\in\mathcal{A}_c} y_d^{\mathrm{ck}} \leq 0 \quad \forall d \in \mathbb{D}. \quad (10)$$

Subtour Elimination Constraints:

$$\sum_{l_1\in\{1\dots\kappa\}} \sum_{l_2\in\{1\dots\kappa\}} \sum_{(i,j)\in\delta_c^+(\mathcal{P})} x_{ij}^{\mathrm{ckl}_1 l_2} \geq 1 + \sum_{i\in\mathcal{P}} \left(y_i^{\mathrm{ck}} - 1\right) \quad \forall c \in \mathcal{C},\ k \in \mathcal{A}_c,\ \mathcal{P} \subseteq V_c \setminus s_c^k. \quad (11)$$

Coverage Constraints:

$$\sum_{c\in\mathcal{C}} \sum_{k\in\mathcal{A}_c} \sum_{i\in\gamma_c(v)} y_i^{\mathrm{ck}} \geq 1 \quad \forall v \in \nu. \quad (12)$$

Refueling Constraints:

$$\sum_{l_2\in\{1\dots\kappa\}} \sum_{j\in V_c} z_{ij}^{\mathrm{ckl}_1 l_2} - \sum_{l_2\in\{1\dots\kappa\}} \sum_{j\in V_c} z_{ji}^{\mathrm{ckl}_2 l_1} = \sum_{l_2\in\{1\dots\kappa\}} \sum_{j\in V_c} \alpha_{ij}^c \cdot x_{ij}^{\mathrm{ckl}_1 l_2} \quad \forall c \in \mathcal{C} \setminus c_0,\ k \in \mathcal{A}_c,\ i \in \mathcal{V}_c,\ l_1 \in \{1 \dots \kappa\} \quad (13)$$

$$z_{di}^{\mathrm{ckl}_1 l_2} = \alpha_{di}^c \cdot x_{di}^{\mathrm{ckl}_1, l_2} \quad \forall c \in \mathcal{C} \setminus c_0,\ k \in \mathcal{A}_c,\ l_1, l_2 \in \{1 \dots \kappa\},\ d \in \mathbb{D},\ i \in V_c \quad (14)$$

$$z_{ij}^{\mathrm{ckl}_1 l_2} \leq (U - \min_{d\in\mathbb{D}} \alpha_{jd}^c) \cdot x_{ij}^{\mathrm{ckl}_1 l_2} \quad \forall c \in C \setminus c_0,\ k \in \mathcal{A}_c,\ l_1, l_2 \in \{1 \dots \kappa\},\ i, j \in V_c. \quad (15)$$

Variable Domain Constraints:

$$x_{ij}^{\mathrm{ckl}_1 l_2} \in \{0, 1\} \quad \forall c \in \mathcal{C},\ k \in \mathcal{A}_c,\ l_1, l_2 \in \{1 \dots \kappa\},\ i, j \in V_c \quad (16)$$

$$y_i^{\mathrm{ck}} \in \{0, 1\} \quad \forall c \in \mathcal{C},\ k \in \mathcal{A}_c,\ i \in V_c \quad (17)$$

$$w_d \in \{0, 1\} \quad \forall d \in \mathbb{D} \quad (18)$$

$$z_{ij}^{\mathrm{ckl}_1, l_2} \in [0, U] \quad \forall c \in \mathcal{C} \setminus c_0,\ k \in \mathcal{A}_c,\ l_1, l_2 \in \{1 \dots \kappa\},\ i, j \in V_c. \quad (19)$$

The objective function [see(2)] combines the length of the kernel of the persistent mission and the setup costs for opening refueling depots in the environment. This helps to jointly optimize the overall cost of the mission. Constraint (3) is a set of degree constraints that ensures that the result is a closed walk. Constraints (4) and (5) together ensure that no viewpoint is visited more than κ number of times. We note that the number of variables, and consequently the size of the search space, increases significantly, with a small increase in the value of κ. Hence, it is to our advantage to restrict its value ($\kappa = 2$), as discussed in Section III-C. Constraints (6)–(8) populate visit variables for viewpoints and depots. Constraints (9) and (10) restrict the placement and number of refueling depots opened in the environment. Constraint (11) ensures that there does

not exist a disconnected subtour unreachable from the starting point (s_c^k). Constraint (12) ensures that for each visibility segment v, at least one viewpoint in the set $\gamma(v)$ is visited by one of the vehicles, thus ensuring coverage. Constraints (13) and (14) ensure fuel conservation at the viewpoints and when traveling out of a depot, respectively. Constraint (15) makes sure that the aerial robot has enough fuel to reach the nearest depot. Constraints (16)–(19) specify the domain for decision variables used in the formulation.

Branch-and-Cut Algorithm

It may be observed that the number of subtour elimination constraints is exponential in the number of viewpoints. It is not computationally efficient to enumerate them all and add to the solver. To address this issue, we use a branch-and-cut framework that works as follows; we solve a relaxed version of the problem that does not include the subtour elimination constraints. When the solver obtains an integer feasible solution to this relaxed problem, we check whether the feasible solution violates any of these constraints. If so, we add the violated constraints to the formulation and continue solving the problem. This process of adding constraints to the problem sequentially has been observed to be computationally efficient for many variants of TSP [39] and fuel constrained vehicle routing problems [13], [30].

The algorithm to identify violated constraints is called a separation algorithm. We present pseudocode for a separation algorithm in Algorithm 1. The procedure computes the connected components in the graph defined by the integer solution for each vehicle. Each component P of cardinality greater than one that satisfies the condition $P \subseteq \mathcal{V}_c \setminus \{s_c^k\}$, where c is the curve on which the kth vehicle traverses and s_c^k is the starting point of the vehicle, violates the corresponding constraint (Constraint (11)). The violated constraints are then added to the formulation, and the solver is allowed to optimize the problem with the new set of constraints.

Algorithm 1 Separation Algorithm

```
for all c ∈ C do
  for all k ∈ A_c do
    Build graph G(directed) ≡ (V = V_c, E)
    Add edge (i, j) to E, if ∃_{l1,l2∈{1...κ}} x_ij^{ckl1l2} = 1
    Find connected components in G
    for all connected components G ∈ G do
      if (|G| > 1)&&(G ⊆ V_c \ s_c^k) then
        Add violation constraint (Eq. (11))
```

B. Construction Heuristic

Due to the computational hardness of HWPRPT, we cannot hope for an exact method such as the MILP-based branch-and-cut algorithm to scale well. In this light, we discuss the design of a computationally efficient heuristic that may be used to compute feasible solutions quickly. The construction heuristic, named δ-search algorithm, is based on the competitive construction of robot paths using a step-increment strategy.

Algorithm 2 δ-Search

```
1: initialize robot paths to starting locations
2: initialize segment coverage vector
3: while all segments are not covered do
4:     for all robots do
5:         compute-Δ-path
6:     δ-increment = minimum cost Δ-path
7:     update robot paths and coverage data
8: return robot paths
```

Algorithm 2 gives pseudocode for δ-search algorithm. It has an iterative construction and incrementally builds robot paths until all segments are covered. The paths are competitively allowed a δ-increment in every iteration based on the value of a cost function. The cost function accounts for distance traveled (fuel consumed), new visibility segments covered, and refueling cost in the case of aerial robots.

Lemma 11: The set of viewpoints on a ground robot's path (tour) that begins and ends at a given starting location on the 1.5-D terrain can be ordered in nondecreasing sequence based on their x-coordinate values.

Proof: The viewpoints visited by a ground robot lie on the 1.5-D terrain. A 1.5-D terrain representation is a x-monotone curve. Hence, the set of all viewpoints on a ground robot's path can be ordered in a nondecreasing sequence. □

Lemma 12: The set of viewpoints on an aerial robot's path (tour) that begins and ends at a given starting location on the terrain can be ordered in nondecreasing sequence based on their x-coordinate values.

Proof: The viewpoints on an aerial robot's path lie on the constant-altitude flight path that is parallel to the x-axis and is x-monotone. Hence, the set of all viewpoints on an aerial robot's path can be ordered in a nondecreasing sequence. □

The δ-search algorithm (see Algorithm 2) works as follows. Each robot path is initialized to the given starting location. Segment coverage vector is initialized and updated to include segments covered by the ground robots at their starting locations. A while loop is used (lines 3–7) to incrementally build robot paths until all visibility segments are covered in combination by the robots. Within each iteration of the while loop, a Δ-path is computed for each robot using the algorithmic routine given in Algorithm 3. The Δ-path with the minimum cost is then marked as the δ-increment. Δ-paths are compared based on the following cost function:

$$\text{cost}(\Delta_i) = d_{\text{cost}}(i) + r_{\text{cost}}(i) + v_{\text{rd}}(i) \tag{20}$$

where Δ_i refers to the Δ-path for robot i, *cost*(Δ_i) is the value of cost function for Δ_i, $d_{\text{cost}}(i)$ corresponds to length of Δ_i (fuel consumed), $r_{\text{cost}}(i)$ corresponds to the cost of refueling visits on Δ_i, and $v_{rd}(i)$ is the visibility score for Δ_i. $v_{rd}(i)$ is inversely proportional to the number of previously uncovered visibility segments covered by Δ_i. If a valid Δ-path for an aerial robot is not found, its d_{cost} value is set to ∞. In the case of ground robots, there always exists a valid Δ-path.

The δ-increment is then added to the corresponding robot's path. Segment coverage vector is updated to include

new segments covered by the δ-increment. The while loop continues until all segments are covered. This ensures that the δ-search algorithm terminates with a valid set of paths for each robot and ensures that each visibility segment is covered.

We now describe the Δ-path computation using the algorithmic routine given in Algorithm 3. It follows from the results in Lemmas 11 and 12 that there always exists a leftmost viewpoint (smallest x-coordinate) and a rightmost viewpoint (largest x-coordinate) on a robot's path at any stage of the algorithm. We call these viewpoints as end viewpoints. To compute the Δ-path, end viewpoints on the robot's path, Π, are identified. Next, a neighbor (adjacent) viewpoint not currently on the robot's path is computed for each end viewpoint. A Δ-path is defined as the path that starts at an end viewpoint, visits the neighbor viewpoint, and then ends at the same end viewpoint while also satisfying the fuel constraint of the robot at every point on the path.

Algorithm 3 Compute-Δ-Path

1: Π = current robot path
2: E_Π = end-viewpoints of Π
3: $N_\Pi = \{n_i$: neighbor viewpoint of $e_i \in E_\Pi$, $n_i \notin \Pi\}$
4: **for all** $e_i \in E_\Pi$ **do**
5: $\quad \Delta_i = \{\phi\}, v_i = \{\phi\}$
6: $\quad length(\Delta_i) = \infty$
7: $\quad \Delta_i^{ab}$ = path from e_i to n_i
8: $\quad \Delta_i^{ba}$ = path from n_i to e_i
9: $\quad$ **if** (Δ_i^{ab} exists) && (Δ_i^{ba} exists) **then**
10: $\quad\quad \Delta_i = \Delta_i^{ab} + \Delta_i^{ba}$
11: $\quad\quad v_i$ = new segments covered by Δ_i
12: $\quad\quad$ Compute $length(\Delta_i)$
13: maxID = $\text{argmax}_{i:e_i \in E_\Pi} \left\{|v_i|/length(\Delta_i)\right\}$
14: **return** Δ_{maxID}

Δ-path construction is done in two steps: 1) from end viewpoint to the neighbor viewpoint and 2) from neighbor viewpoint back to end viewpoint. The computation is shown in the for loop (lines 4–12) in Algorithm 3 and works as follows. For ground robots, the Δ-path computation is straightforward and is computed as point-to-point traversals. In the case of aerial robots, the path computation in step 1 must account for the amount of fuel left in the robot when it reaches the end viewpoint and the fuel required to reach the neighbor viewpoint. For path computation in step 2, the amount of fuel left when the robot completes the return journey to the end viewpoint must be sufficient to reach the next refueling depot or return to the starting depot, as the case may be, on the original path. In both cases, if point-to-point paths satisfy fuel constraints, the paths are computed as direct traversals. Otherwise, we find the minimum cost traversal that includes a refueling visit to the nearest refueling depot. Any Δ-paths and the resultant robot paths computed in this way satisfy fuel constraints. We restrict our search of Δ-paths to include at most one refueling visit on each step of the path between an end viewpoint and its neighbor. This choice was observed to perform well while still being computationally tractable. Utility value for a Δ-path is computed as the number of new visibility segments covered per unit length (line 13 in Algorithm 3). The path that maximizes the utility function is returned to the δ-search algorithm as the robot's Δ-path.

TABLE I
SIMULATION PARAMETERS USED FOR INSTANCE GENERATION

S.No.	Parameter Name	# values used	Range of Values
1	size (# terrain points)	4	$\{5, 10, 15, 20\}$
2	1.5D terrain	20	random
3	starting location	5	random
4	fuel capacity	5	see Table II

VI. COMPUTATIONAL SIMULATIONS

A synthetic simulation platform was built to study and analyze the computational efficiency of the developed approaches. In the following, we discuss the simulation setup, instance generation, a few sample scenarios, and results of computational simulations.

A. Simulation Setup

The MILP formulation requires significant computational resources. Therefore, the simulations were performed on a High Performance Cluster running Cent OS 6.5. Two blade servers within the cluster, each with 20 cores and 96-GB RAM, were used. The number of cores assigned to each process was dynamically decided by the HPC scheduler and was not fixed. The MILP formulation was implemented in C++ using IBM ILOG CPLEX library version 12.7. The branch-and-cut framework was implemented using solver callback (lazy callbacks) functionality of the CPLEX library and LEMON graph library. For each instance, the solver was allowed to execute for 3600 s or up to 1% relative gap, whichever was reached first. Relative gap of a solution is defined as $((x - lb)/lb) * 100$, where x is the cost of the computed solution and "lb" is the best lower bound found so far.

B. Instance Generation

The simulations were executed for a total of 2000 randomly generated instances. The values of various simulation parameters are summarized in Table I. Size of the environment in terms of terrain points was varied from 5 to 20 in steps of 5. For each environment size, 20 random 1.5-D terrains were generated. A total of six robotic sensor nodes were made available for each run: two ground robots and four aerial robots. For each environment, five different starting locations were generated randomly for each robot. Some sample instances used in the simulation are shown in Fig. 4 along with the routes computed by the MILP solver. The starting locations were chosen randomly from the reflex points on the terrain. Refueling depot opening sites were placed at each of the reflex points. The total width of the terrain was fixed at 1000 units. The terrain point altitudes were generated within the range 0–1300 units. The two aerial robots were operated at 1500 units altitude (A1) and 1800 units altitude (A2). The fuel capacity (U_k^c) for the aerial robots was selected from five

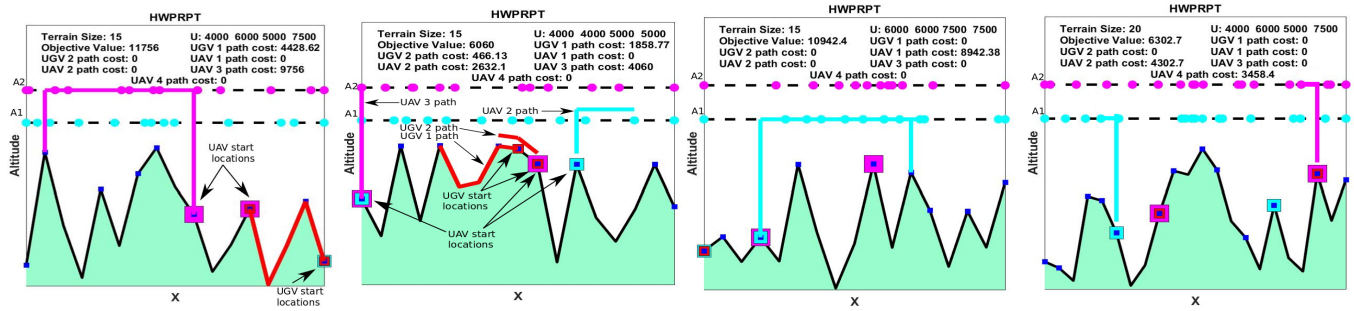

Fig. 4. Sample instances from the simulation set. The paths are color-coded. Red color represents ground robots, cyan color represents robots flying at altitude 1, and magenta color represents aerial robots flying at altitude 2. Blue squares represent refueling depot opening sites. Starting location for the robots is shown in concentric hollow squares on the reflex points in the corresponding color. The size of these squares increases with increase in the robot's operating altitude. (a) Example instance where one UAV and one UGV are used. (b) Example instance where two UAVs and UGVs are used. The UAVs are deployed at different altitudes. (c) Example instance where one UAV is used. (d) Example instance where two UAVs are used.

TABLE II

FUEL CAPACITIES (U_k^c) FOR UAVS. UAVS 1 AND 2 WERE OPERATED AT ALTITUDE 1500 UNITS. UAVS 3 AND 4 WERE OPERATED AT ALTITUDE 1800 UNITS

S.No.	UAV 1	UAV 2	UAV 3	UAV 4
1	2000	2000	2500	2500
2	2000	4000	2500	5000
3	4000	4000	5000	5000
4	4000	6000	5000	7500
5	6000	6000	7500	7500

TABLE III

COSTS FOR DIFFERENT VEHICLES

Ground Robot Path Cost	distance × costFactor where, costFactor (uphill) = $1 + \frac{\theta}{\pi/2} \times \bar{\gamma}$ costFactor (downhill) = $1 + \frac{\theta}{\pi/2} \times \underline{\gamma}$
Aerial Robot Path Cost	takeoff/landing cost = 2× distance horizontal travel cost = distance × costFactor where, costFactor = $2 + (A_i/\bar{A})$

pregenerated sets of values, as shown in Table II. Note that in the case of ground robots, the cost is proportional to both the distance traveled and the slope of the terrain, as mentioned in Section III-B. The ground robots incur an additional cost depending on the slope defined as an uphill travel coefficient, $\bar{\gamma} = 0.35$, and a downhill travel coefficient, $\underline{\gamma} = -0.15$. Aerial robot cost computation uses the following parameters, A_i, $\forall i \in \{1 \ldots (|\mathcal{C}| - 1)\}$ and $\bar{A} = 2000$ units, where A_i is the flight altitude and $\bar{A}$ represents the maximum permissible altitude. The cost of opening a refueling depot is fixed at 1000 units. The cost computation for ground robots and aerial robots is shown in Table III.

C. Illustrative Scenarios

Before considering the simulation results, we will show how the paths for the robotic sensors are generated by our planner to perform monitoring on a terrain. Fig. 4 shows a few sample instances and the robot paths computed by the MILP solver. The robots available for monitoring are: two ground robots (UGVs 1 and 2), two aerial robots (UAVs 1 and 2) at altitude A1, and two aerial robots (UAVs 3 and 4) at altitude A2. The ground robot paths are shown in red lines. Paths for aerial robots at altitude A1 are shown in cyan color, whereas magenta-colored paths represent UAVs 3 and 4 at altitude A2. To distinguish the paths of UGV 2, UAV 2, and UAV 4 from other robots operating at the same altitude, namely UGV 1, UAV 1, and UAV 3, respectively, we add a small vertical offset in the visualization. Refueling depot opening sites are shown in small blue squares. Starting location for the robots is shown in concentric hollow squares on the reflex points in the corresponding color. The size of these squares increases with increase in the robot's operating altitude.

Consider the 1.5-D terrain shown in Fig. 4(a). The terrain consists of nine reflex points. The fuel capacities U_k^c for the UAVs are mentioned within the figure following the letter U. The robot operating costs were computed, as given in Table III. The route determined by the proposed MILP solution is shown in Fig. 4(a). In this scenario, only UGV 1 and UAV 3 at altitude A2 are utilized. The cost incurred by individual robots is shown in Fig. 4(a). These two robots persistently monitor the terrain by operating on the assigned routes. The solution makes use of two refueling depots whose opening costs equal $2*1000$ units. The objective value mentioned in the figure reports the total cost of the operation, as given by (2). In this instance, it includes the opening cost of two refueling depots (2000 units) and the maximum operating cost of a robot (9756 units), thus making a total of 11 756 units.

Consider another scenario as shown in Fig. 4(b). The environment consists of 17 terrain points and nine reflex points. In this case, two aerial robots (UAV 2 at A1 and UAV 3 at A2 altitudes) and two UGVs were used to monitor the terrain. UAV 3 must hover above its take-off location at altitude A2 so that the combined visibility of the agents covers the terrain.

The next example, shown in Fig. 4(c), uses only one aerial robot (UAV 1) for monitoring. The scenario consists of 16 terrain points and nine reflex points. In the scenario shown in Fig. 4(d), two aerial robots (UAVs 2 and 4) are used at different altitudes to monitor. The example has 22 terrain

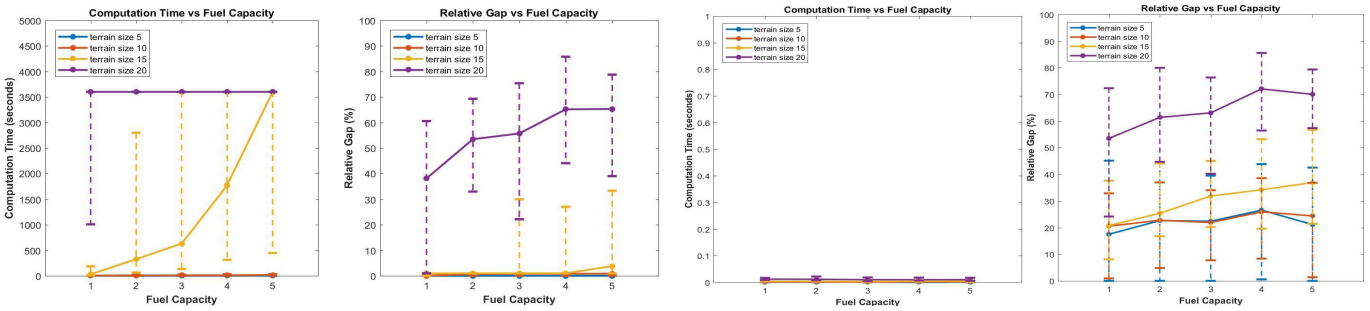

Fig. 5. Effect of change in fuel capacities (fuel capacity serial IDs correspond to serial numbers in Table II) in terms of computation time and relative gap of the best solution computed by the solver within 3600 s for (a) and (b) MILP approach and (c) and (d) heuristics algorithm.

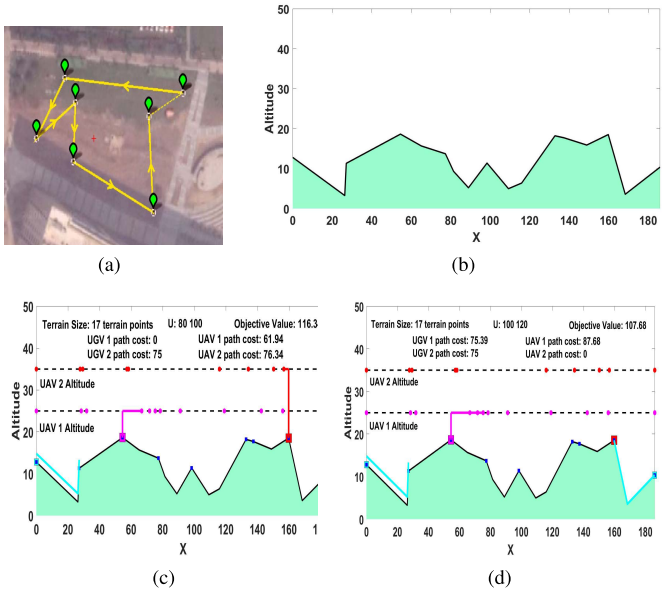

Fig. 6. (a) Simulated pathlike feature used in the experiments. (b) 1.5-D terrain superimposed on the feature. (c) and (d) Robot paths generated by the MILP solver for experiments 1 and 2, respectively. Ground robot paths are shown in cyan color lines. Aerial robot #1 and #2 paths are shown in magenta and red color lines, respectively. The starting locations for the robots are shown as large hollow squares of the corresponding color. Refueling station opening sites are shown in small blue squares.

points and 13 reflex points. These examples showed how the paths for different vehicles are determined for monitoring. The generated paths depend on the terrain profile, robot operating and travel costs, fuel levels, operating altitudes, and the placement of refueling depots. When these parameters are modified, the optimal cost and routes will also change.

D. Results

We will now analyze the effect of different fuel capacity and number of terrain points when using the MILP formulation and heuristics for the simulation instances described in Section V-A. Fig. 5(a) shows the computation time taken by the solver as median values along with the first and third quartiles. Fig. 5(b) shows the relative gap for the best solution computed by the MILP solver within the time limit (3600 s). The plots show a distinctive correlation. The values for large environment size (terrain size with 20 terrain points) have high time consumption and relative gap. This is a consequence of

TABLE IV

NUMBER OF INSTANCES SOLVED OPTIMALLY BY THE MILP SOLVER. NUMBERS IN BRACKETS REPRESENT THE INSTANCES FOR WHICH THE SOLVER COULD FIND AT LEAST ONE FEASIBLE SOLUTION BUT NOT OPTIMAL

Instance Size	# instances solved optimally
5	500(0)
10	491(9)
15	334(166)
20	73(420)

exponential increase in the size of the MILP formulation with an increase in instance size, and hence, the solver is not able to compute the optimal solution for most instances.

The results of computational simulations for the construction heuristic are shown in Fig. 5(c) and (d). Fig. 5(c) shows the time taken to compute the solution against fuel capacity for the various instance sizes. We observe that computation time taken to compute solutions for instances of all sizes and fuel capacity values is less than 1 s. The heuristic has a very low computational time requirement. However, as shown in Fig. 5(d), which shows the median relative gap for solution computed by the heuristic algorithm, the tradeoff results in a drop in solution quality. The heuristic is thus useful in cases where computation time is of importance. It can also be used as an initial feasible solution to the MILP solver.

The number of instances solved optimally by the MILP solver is reported in Table IV. It also reports the number of instances for which the solver found a feasible solution, but it was unable to prove optimality within the given time limit. Adding up the numbers for each instance size, we observe that for instances with 20 terrain points, the solver could not find any solution for seven instances within the stipulated time. An increase in computation time (for instances solved optimally) and declination in solution quality within the given time limit is also observed with an increase in fuel capacity (see Fig. 5). This is attributed to the increase in search space with increasing values of fuel capacity.

VII. PROOF-OF-CONCEPT EXPERIMENTS

The solution methods proposed for coverage of a piecewise linear feature with load balancing and placement of refueling depots were also demonstrated in proof-of-concept experiments. Due to limited resources, the experiments were

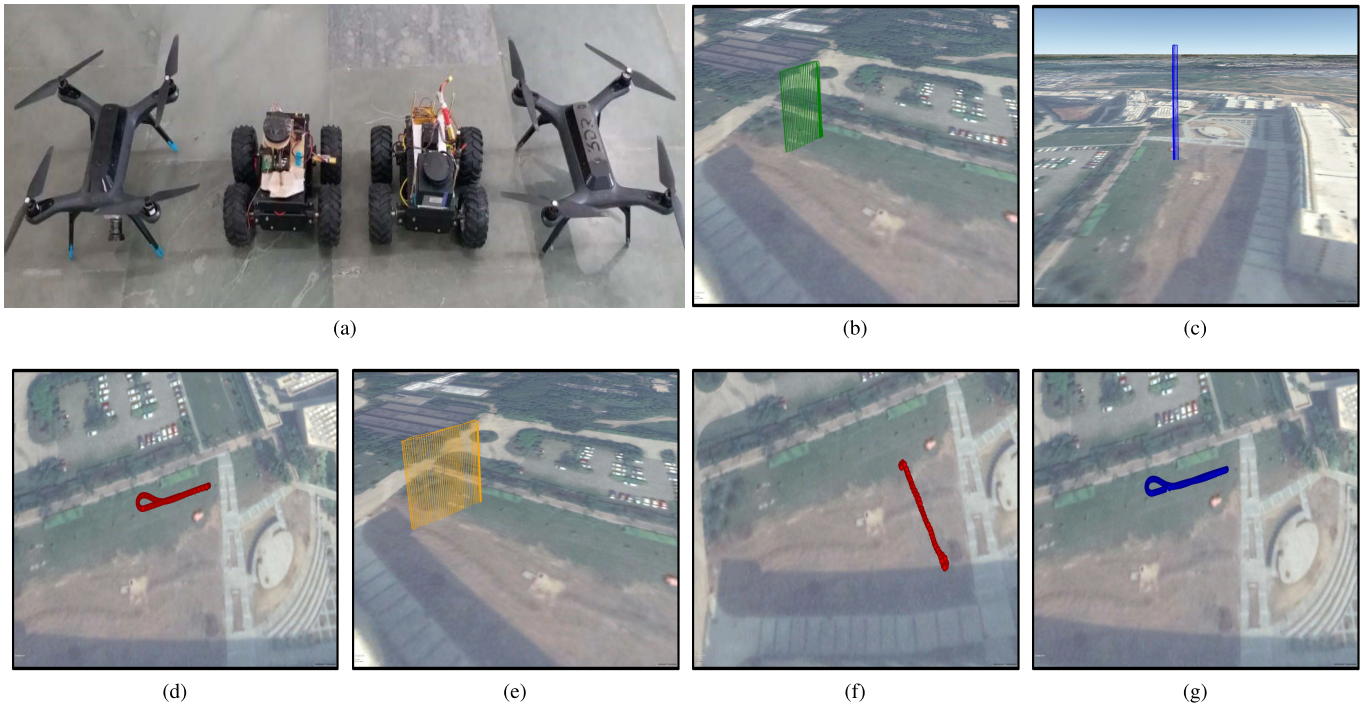

Fig. 7. (a) Robots used for the experiment. (b)–(g) Paths traversed by individual robots in the experiments. The paths were traced out using telemetry data collected during the robot mission. Visualizations were done in Google Earth Pro software. The paths also show the altitude profile for the aerial robots. (b)–(d) Paths traversed by UAV #1, UAV #2, and UGV #2 during experiment 1. (e)–(g) Paths traversed by UAV #1, UGV #1, and UGV #2 during experiment 2.

conducted within the university campus at IIIT Delhi using four robots: two aerial robots and two ground robots. A simulated piecewise linear feature as shown in Fig. 6(a) was superimposed on the terrain shown in Fig. 6(b) to build the experimental setup. The operational region was of size $\sim 80 \times 60$ m^2 and the length of the simulated feature was $\sim$188 m. We computed paths for the robots using the MILP-based solver [see Fig. 6(c) and (d)]. The proof-of-concept demonstration holds importance since it shows the feasibility of the kernel computed by the solver for the persistent mission. The optimal placement of refueling depots and the planned routes ensure that the aerial robots never run out of fuel and can sustain the persistent mission. The experiments illustrate that even with purely offline planning based on the geometry of the terrain and cost models for the robots, our methods can be used in real implementations.

Two 3DR Solo quad-copters were used as aerial robots in the experiments [see Fig. 7(a)]. They were operated using the ArduCopter firmware and employed at 25 m (id #1) and 35 m (id #2) altitude. Both the aerial robots were set to a cruise speed of 1 m/s and vertical speed (during take-off and landing) of 1 m/s. Aerial robot operating cost was directly proportional to the distance traveled, and the constant of proportionality was based on flight altitude. The ground robots were custom built using Pixhawk cube flight controllers and used the ArduRover firmware. They were also operated at a speed of 1 m/s. The ground robot operating cost was proportional to the distance traveled and slope of the terrain. All costs were computed in terms of fuel consumption.

Two sets of experiments were conducted. The simulator visualization of robot paths generated for the experiment is shown in Fig. 6(c) and (d). The flight range of aerial robots, U, was varied over the two experiments. The set of values used was (80, 100) in experiment 1 and (100, 120) in experiment 2. The refueling depot opening cost was fixed at 30 units. The first experiment utilized both the aerial robots and one ground robot. The exact paths traversed by the robots as traced using the telemetry logs from the robots and visualized in Google Earth are shown in Fig. 7(b)–(d). In the second experiment, one aerial robot and both ground robots were used. The robot paths captured using telemetry data and visualized in Google Earth are shown in Fig. 7(e)–(g). The experiment video showing complete mission operation for both the experiments may be viewed in the multimedia attachment.

VIII. Conclusion

In this work, we address the persistent monitoring problem on piecewise linear features on terrains. We have developed methods for the use of a heterogeneous set of aerial and ground robotic sensors. The MILP formulation-based implementation allows the computation of exact solutions for smaller instances of the problem. For larger instances, we design fast construction heuristics to compute feasible solutions. We evaluate and analyze our methods in simulation and also show experiment demonstrations, albeit using a virtually simulated terrain. The experiments demonstrate the proof of concept for persistent monitoring operations in a limited outdoor setting.

This work opens up avenues for future extension. There is a need to develop approximation algorithms that have bounds on the quality of the solution. It would also be interesting to evaluate the performance of evolutionary heuristics that speed up MILP computations for this problem since the search space size increases very quickly with large instances.

The exact solution to the 2.5-D version of the problem for coverage on terrains is also an open problem and is very challenging. Another interesting extension is to take uncertainty into account while planning the route for the vehicles. The uncertainty could be from the perceived information or vehicle failures or dynamically changing environment.

ACKNOWLEDGMENT

The authors would like to thank G. Gupta and K. Yu for help with the preliminary work on this article.

REFERENCES

[1] S. G. Manyam, S. Rasmussen, D. W. Casbeer, K. Kalyanam, and S. Manickam, "Multi-UAV routing for persistent intelligence surveillance & reconnaissance missions," in *Proc. IEEE Int. Conf. Unmanned Aircr. Syst.*, Jun. 2017, pp. 573–580.

[2] W. H. Chun and N. Papanikolopoulos, "Robot surveillance and security," in *Springer Handbook of Robotics* (Springer Handbooks). Cham, Switzerland: Springer, 2016, pp. 1605–1626.

[3] R. R. Murphy, *Disaster Robotics*. Cambridge, MA, USA: MIT Press, 2014.

[4] H. Ghazzai, A. Kadri, M. B. Ghorbel, and H. Menouar, "Optimal sequential and parallel UAV scheduling for multi-event applications," in *Proc. IEEE 87th Veh. Technol. Conf. (VTC Spring)*, Jun. 2018, pp. 1–6.

[5] K. Máthé and L. Buşoniu, "Vision and control for UAVs: A survey of general methods and of inexpensive platforms for infrastructure inspection," *Sensors*, vol. 15, no. 7, pp. 14887–14916, Jun. 2015.

[6] N. Lasla, H. Ghazzai, H. Menouar, and Y. Massoud, "Exploiting land transport to improve the UAV's performances for longer mission coverage in smart cities," in *Proc. IEEE 89th Veh. Technol. Conf. (VTC-Spring)*, Apr. 2019, pp. 1–7.

[7] E. Resendiz, J. Hart, and N. Ahuja, "Automated visual inspection of railroad tracks," *IEEE Trans. Intell. Transp. Syst.*, vol. 14, no. 2, pp. 751–760, May 2013.

[8] J. Katrasnik, F. Pernus, and B. Likar, "A survey of mobile robots for distribution power line inspection," *IEEE Trans. Power Del.*, vol. 25, no. 1, pp. 485–493, Jan. 2010.

[9] A. Ryan *et al.*, "A modular software infrastructure for distributed control of collaborating UAVs," in *Proc. AIAA Guid., Navigat., Control Conf.*, Aug. 2006, p. 6455.

[10] S. Rathinam *et al.*, "Autonomous searching and tracking of a river using an UAV," in *Proc. Amer. Control Conf.*, Jul. 2007, pp. 359–364.

[11] S. Rathinam, Z. W. Kim, and R. Sengupta, "Vision-based monitoring of locally linear structures using an unmanned aerial vehicle," *J. Infrastruct. Syst.*, vol. 14, no. 1, pp. 52–63, Mar. 2008.

[12] R. W. Beard, T. W. McLain, D. B. Nelson, D. Kingston, and D. Johanson, "Decentralized cooperative aerial surveillance using fixed-wing miniature UAVs," *Proc. IEEE*, vol. 94, no. 7, pp. 1306–1324, Jul. 2006.

[13] P. Maini, K. Sundar, M. Singh, S. Rathinam, and P. B. Sujit, "Cooperative aerial–ground vehicle route planning with fuel constraints for coverage applications," *IEEE Trans. Aerosp. Electron. Syst.*, vol. 55, no. 6, pp. 3016–3028, Dec. 2019.

[14] K. Yu, A. K. Budhiraja, S. Buebel, and P. Tokekar, "Algorithms and experiments on routing of unmanned aerial vehicles with mobile recharging stations," *J. Field Robot.*, vol. 36, no. 3, pp. 602–616, May 2019.

[15] S. G. Manyam, K. Sundar, and D. W. Casbeer, "Cooperative routing for an air-ground vehicle team—Exact algorithm, transformation method, and heuristics," *IEEE Trans. Autom. Sci. Eng.*, vol. 17, no. 1, pp. 537–547, Aug. 2019.

[16] N. Mathew, S. L. Smith, and S. L. Waslander, "Multirobot rendezvous planning for recharging in persistent tasks," *IEEE Trans. Robot.*, vol. 31, no. 1, pp. 128–142, Feb. 2015.

[17] P. Tokekar and V. Kumar, "Visibility-based persistent monitoring with robot teams," in *Proc. IEEE/RSJ Int. Conf. Intell. Robots Syst. (IROS)*, Sep. 2015, pp. 3387–3394.

[18] S. Alamdari, E. Fata, and S. L. Smith, "Persistent monitoring in discrete environments: Minimizing the maximum weighted latency between observations," *Int. J. Robot. Res.*, vol. 33, no. 1, pp. 138–154, Jan. 2014.

[19] P. Maini and P. B. Sujit, "On cooperation between a fuel constrained UAV and a refueling UGV for large scale mapping applications," in *Proc. Int. Conf. Unmanned Aircr. Syst. (ICUAS)*, Jun. 2015, pp. 1370–1377.

[20] F. Ropero, P. Muñoz, and M. D. R-Moreno, "Terra: A path planning algorithm for cooperative UGV–UAV exploration," *Eng. Appl. Artif. Intell.*, vol. 78, pp. 260–272, Feb. 2019.

[21] W. Chin and S. Ntafos, "Optimum watchman routes," in *Proc. Symp. Comput. Geometry (SCG)*, New York, NY, USA, 1986, pp. 24–33.

[22] X. Tan, "Fast computation of shortest watchman routes in simple polygons," *Inf. Process. Lett.*, vol. 77, no. 1, pp. 27–33, Jan. 2001.

[23] J. S. B. Mitchell, "Approximating watchman routes," in *Proc. Symp. Discrete Algorithms*. Philadelphia, PA, USA: Society for Industrial and Applied Mathematics, Jan. 2013, pp. 844–855.

[24] S. Carlsson, H. Jonsson, and B. J. Nilsson, "Finding the shortest watchman route in a simple polygon," *Discrete Comput. Geometry*, vol. 22, no. 3, pp. 377–402, Oct. 1999.

[25] E. Packer, "Computing multiple watchman routes," in *Experimental Algorithms* (Lecture Notes in Computer Science), vol. 5038. Berlin, Germany: Springer, 2008, pp. 114–128.

[26] J. Faigl, "Approximate solution of the multiple watchman routes problem with restricted visibility range," *IEEE Trans. Neural Netw.*, vol. 21, no. 10, pp. 1668–1679, Oct. 2010.

[27] B. J. Nilsson and D. Wood, "Optimum watchmen routes in spiral polygons," in *Proc. Can. Conf. Comput. Geometry*, 1990, pp. 269–272.

[28] S. Carlsson, B. J. Nilsson, and S. Ntafos, "Optimum guard covers and m-watchmen routes for restricted polygons," in *Proc. Workshop Algorithms Data Struct.* Berlin, Germany: Springer, 1991, pp. 367–378.

[29] K. Kalyanam, S. Manyam, A. Von Moll, D. Casbeer, and M. Pachter, "Scalable and exact MILP methods for UAV persistent visitation problem," in *Proc. IEEE Conf. Control Technol. Appl. (CCTA)*, Aug. 2018, pp. 337–342.

[30] K. Sundar and S. Rathinam, "Algorithms for routing an unmanned aerial vehicle in the presence of refueling depots," *IEEE Trans. Autom. Sci. Eng.*, vol. 11, no. 1, pp. 287–294, Jan. 2014.

[31] S. K. K. Hari, S. Rathinam, S. Darbha, K. Kalyanam, S. G. Manyam, and D. Casbeer, "The generalized persistent monitoring problem," in *Proc. Amer. Control Conf. (ACC)*, Jul. 2019, pp. 2783–2788.

[32] N. Mathew, S. L. Smith, and S. L. Waslander, "Planning paths for package delivery in heterogeneous multirobot teams," *IEEE Trans. Autom. Sci. Eng.*, vol. 12, no. 4, pp. 1298–1308, Oct. 2015.

[33] K. Yu, J. M. O'Kane, and P. Tokekar, "Coverage of an environment using energy-constrained unmanned aerial vehicles," in *Proc. Int. Conf. Robot. Automat. (ICRA)*, May 2019, pp. 3259–3265.

[34] S. Funke, A. Nusser, and S. Storandt, "Placement of loading stations for electric vehicles: No detours necessary!" *J. Artif. Intell. Res.*, vol. 53, pp. 633–658, Aug. 2015.

[35] P. Maini, G. Gupta, P. Tokekar, and P. B. Sujit, "Visibility-based monitoring of a path using a heterogeneous robot team," in *Proc. IEEE/RSJ Int. Conf. Intell. Robots Syst. (IROS)*, Oct. 2018, pp. 3765–3770.

[36] P. Maini, K. Yu, P. B. Sujit, and P. Tokekar, "Persistent monitoring with refueling on a terrain using a team of aerial and ground robots," in *Proc. IEEE/RSJ Int. Conf. Intell. Robots Syst. (IROS)*, Oct. 2018, pp. 8493–8498.

[37] S. Carlsson and B. J. Nilsson, "Computing vision points in polygons," *Algorithmica*, vol. 24, no. 1, pp. 50–75, May 1999.

[38] Z. Drezner and H. W. Hamacher, *Facility Location: Applications and Theory*. Berlin, Germany: Springer-Verlag, 2001.

[39] M. Grötschel *et al.*, "Polyhedral theory," in *The Traveling Salesman Problem*. Hoboken, NJ, USA: Wiley, 1985, pp. 251–305.

Parikshit Maini (Member, IEEE) received the B.Tech. degree in information technology from Guru Gobind Singh Indraprastha University, New Delhi, India, in 2012, and the M.Tech. and Ph.D. degrees in computer science and engineering from the Indraprastha Institute of Information Technology Delhi, New Delhi, in 2014 and 2020, respectively.

He is currently a Post-Doctoral Researcher with the Department of Computer Science and Engineering, University of Minnesota, Minneapolis, MN, USA. His research interests include motion planning, multirobot cooperation, and robot learning.

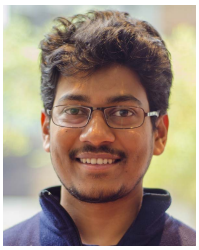

Pratap Tokekar received the Bachelor of Technology degree in electronics and telecommunication from the College of Engineering Pune, Pune, India, in 2008, and the Ph.D. degree in computer science from the University of Minnesota, Minneapolis, MN, USA, in 2014.

He was a Post-Doctoral Researcher with the GRASP Laboratory, University of Pennsylvania, Philadelphia, PA, USA. From 2015 to 2019, he was an Assistant Professor with the Department of Electrical and Computer Engineering, Virginia Tech, Blacksburg, VA, USA. He is currently an Assistant Professor with the Department of Computer Science and the Institute for Advanced Computer Studies, University of Maryland, College Park, MD, USA.

Dr. Tokekar was a recipient of the NSF CAREER Award in 2020 and the CISE Research Initiation Initiative Award in 2016. He serves as an Associate Editor for the IEEE ROBOTICS AND AUTOMATION LETTERS, the IEEE TRANSACTIONS OF AUTOMATION SCIENCE AND ENGINEERING, and the ICRA and IROS Conference Editorial Board.

P. B. Sujit (Senior Member, IEEE) received the bachelor's degree from Bangalore University, Bengaluru, India, in 1998, the master's degree from Visveswaraya Technological University, Bengaluru, in 2002, and the Ph.D. degree from the Indian Institute of Science, Bengaluru, in 2006.

He is currently an Associate Professor with the Indian Institute of Science Education and Research, Bhopal, India. His research interests include unmanned aerial and underwater vehicles, multirobot systems, and human–swarm interaction.